Desalination and Water Treatment
www.deswater.com

doi:10.5004/dwt.2019.24611

166 (2019) 9–23
October

PES/PVDF blend membrane and its composite with graphene nanoplates: preparation, characterization, and water desalination via membrane distillation

Mohamed S. Salem[a,b], Ahmed H. El-Shazly[a,c], Norhan Nady[a,d,*], Mohamed R. Elmarghany[a,b], Mohamed Nabil Sabry[b]

[a]*Chemical and Petrochemicals Engineering Department, Egypt-Japan University of Science and Technology (E-JUST), Alexandria, Egypt, email: mohamedsameh@mans.edu.eg (M.S. Salem), mohamed_ragab@mans.edu.eg (M.R. Elmarghany)*
[b]*Mechanical Power Engineering Department, Faculty of Engineering, Mansoura University, Mansoura, Egypt, email: mnabil.sabry@gmail.com (M.N. Sabry)*
[c]*Chemical Engineering Department, Faculty of Engineering, Alexandria University, Alexandria, Egypt, email: elshazly_a@yahoo.com (A.H. El-Shazly)*
[d]*Polymeric Materials Research Department, City of Scientific Research and Technological Applications (SRTA-city), Borg El-Arab City, Alexandria, Egypt, email: norhan.nady77@yahoo.com (N. Nady)*

Received 2 January 2019; Accepted 24 June 2019

ABSTRACT

One of the major obstacles that hinder commercialization of membrane distillation (MD) for separation applications, especially for water desalination, is the limited adequate low-cost hydrophobic membranes. In this study, a novel poly(ethersulfone)/polyvinylidene fluoride (PES/PVDF) blend membrane and its composite with modified graphene nanoplatelets (GNPs) was fabricated using electro spinning technique. The fabricated pure and blend membranes as well as the composite membranes with GNPs were investigated using scanning electron microscope (SEM), X-ray diffraction analysis (XRD) as well as static water contact angle, liquid entry pressure and membrane porosity measurements. The average fiber diameter and the average membrane pore diameter were estimated using Image J software. A mathematical model was established and utilized to calculate the mass transfer coefficient for the different fabricated membranes at different feed flow rates. Moreover, membranes' MD performances were evaluated using a direct contact membrane distillation unit. The addition of only 2 wt.% GNPs into the PES/PVDF (3:1 w/w) blend increased its water contact angle up to 132.3 ± 0.8°. This composite membrane achieved a flux of about 19.35 kg/m^2·h at feed inlet temperature of 65°C, flow rate of 30 l/h, and salt concentration of 10,000 ppm. The produced PES/PVDF/GNPs composite membrane showed a comparable performance to pure PVDF and PVDF/GNPs composite membranes. Although, a proper economic study is needed, the fact that commercial PES was used, which is relatively cheaper than PVDF, may make the PES/PVDF/GNPs composite membrane a viable candidate for MD applications.

Keywords: Composite membrane, Membrane distillation; Desalination; Poly(ethersulfone)

*Corresponding author.

1. Introduction

In the last few years, global demand for drinkable water has substantially increased, due to population growth. The worldwide demand of fresh water for agricultural, industrial and domestic applications is predicted to reach about 6,900 billion m^3/day by the year 2030, which would surpass the present available fresh water resources by about 40% [1]. As of now, only about 2.53% of worldwide water reserve is fresh water. Around 68.7% of this reserve is trapped in the form of ice in the north and south poles. Salt-water presents the other 97.47% of the water reserve but cannot be directly consumed due to its high saline content. Natural fresh water resources scarcity increases the necessity of searching for alternative means of water supply, like salt-water desalination. With the growing energy and water crises, it is vital to search for pioneering techniques for efficient utilization of unconventional energy sources to face water deficiencies. One of the possible techniques for achieving this goal is membrane distillation (MD).

MD is a thermal membrane separation technique, which employs partial vapor pressure difference generated due to temperature difference across a semipermeable hydrophobic membrane to drive vapor through membrane pores [2–5]. It can be used for desalination, waste water treatment, food industries and numerous other applications [6,7]. The membrane used is usually hydrophobic, which means that it prevents the penetration of liquid but allows vapor to pass through its pores and thus trapping the salt on the other side. There are four primary configurations for MD systems. The simplest and most frequently used configuration is direct contact membrane distillation (DCMD) [8–11], in which water vapor is generated in the hot feed side. Then, the vapor penetrates the membrane pores to the cold permeate side where it condenses by a cold stream. Other MD configurations are air gap membrane distillation (AGMD) [12–14], sweeping gas membrane distillation (SWMD) [15–17], and vacuum membrane distillation (VMD) [18–20]. MD process has numerous benefits over other conventional distillation processes including; the ability to produce high quality distillate at relatively low working pressures, using low temperature differences as a driving force which allows for utilization of low-grade energy resources such as solar energy or waste heat, and low vulnerability to fouling and scaling compared to the other separation processes [21].

A suitable membrane for MD process should exhibit certain qualities such as high hydrophobicity, high vapor flux, low thermal conductivity, and high chemical stability [22]. So far, the most frequently used membrane materials for MD applications are polypropylene (PP) [23], polyvinylidene fluoride (PVDF) [24], and Polytetrafluoroethylene (PTFE) [25], as they exhibit natural hydrophobic qualities. However, exploring novel membranes exclusively for MD applications represents an interesting point of research. Previous efforts for acquiring novel MD membranes were done by using uncommon materials such as ceramic [26], polysulfone [27], polyethylene [28], and metal–organic framework (MOF) [29] to alter their qualities to be better suited for MD applications. Other researchers focused on membrane surface modification. Surface modification generally aims to increase hydrophobicity either by increasing the membrane's surface roughness or by decreasing its surface energy or both. Surface modification can be done using coating [22], plasma treatment [30], or incorporation of some inorganic additives like carbon nanotubes [31,32], Titanium dioxide [33,34], and graphene [28,35]. Other researches presented other preparation techniques such as multi-layer membranes [36] and post-treated membranes [37].

There are several techniques for membrane fabrication for MD process such as phase inversion [24,38,39], and sol-gel [40–42]. Recently, electro spinning technique [36,43–47] has been highlighted as one of the best techniques to obtain high porous membranes suitable for MD process. Electro spinning utilizes high voltage applied to a polymeric solution in a syringe to generate nanofibers that can by collected over a plate or a drum to constitute a nanofibrous membrane. Produced membranes have some favorable advantages such as high surface area to volume ratio, enhanced hydrophobicity, and high porosity. The membrane thickness and pore size can be adjusted by varying the operating conditions such as applied voltage, solution flow rate, syringe movement, process time and distance between the syringe and the collector [48], which makes it relatively easier to fabricate membranes with varying characteristics. Previous researchers used lithium chloride as an additive to the polymeric solution to enhance its polarity and improve the electro-spinning process [49].

Poly(ethersulfone) (PES) is considered one of the promising materials for MD applications. It is a thermoplastic polymer with favorable qualities such as high glass transition temperature, high chemical stability, good mechanical strength, and relatively low price compared to other formerly used materials for MD membranes [50]. PES membranes are widely utilized for microfiltration and ultrafiltration [51–53]. However, due to the presence of ether bonds in their chains, PES membranes have limited hydrophobicity and exhibit a relatively low contact angle. This limits their utilization in MD applications. In order to benefit from the qualities of PES membranes, they must go under some modifications. Some of the previous efforts for modifying PES membranes included, for instance, fluoroalkylsilane treatment [54], plasma treatment [30], incorporating titanium oxide nanotubes in the membrane dope [33, 55], surface grafting [56], and coating using silica nanoparticles and subsequently vacuum filtration coating [57].

One of the promising materials that has been lately utilized to be embedded in the membrane matrix is graphene. Graphene has numerous attractive characteristics like hydrophobicity, ion selectivity, high thermal conductivity, suitable mechanical strength, and high thermal stability [58–60]. Graphene proved to be a good candidate for usage as a membrane filler material for MD applications, as it was found to enhance membrane desirable characteristics beside adding some favorable functionalities like anti-fouling [61].

In this work, a novel composite of PES/PVDF blend with hydrocarbon modified (hydrophobic) graphene nanoplatelets (GNPs) is presented. Electro-spun pure PES, pure PVDF, PES/PVDF blend, PES/GNPs, PVDF/GNPs and PES/PVDF/GNPs composite membranes have been investigated. The prepared membranes were fabricated and characterized using different analysis techniques such as scanning electron microscope (SEM) imaging, X-ray diffraction analysis (XRD), static water contact angle measurements as well as the membrane porosity and the liquid entry

pressure measurements were done. Also, the average fiber diameter and the average membrane pore diameter were calculated using Image J software. The membranes MD performance was investigated using a lab scale direct contact membrane distillation unit under different conditions.

2. Experimental

2.1. Materials

Commercial PES Ultrason E 6020P flakes (ρ = 1.37 g/ cm^3 and M_w = 46,000–55,000 g/mol) were provided by BASF, Germany. Polyvinylidene fluoride (PVDF) pellets (ρ = 1.78 g/ cm^3 and M_w = 275,000 g/mol) and functionalized, hydrocarbon modified (hydrophobic) graphene nanoplatelets (GNPs) (> 85% C, ρ = 0.04 g/mol and M_w = 12.01 g/ mol) were supplied by Sigma-Aldrich, USA. As for the solvents; N, N-Dimethylformamide (DMF) (> 99.8% C_3H_7NO, HPLC grade, ρ = 1.4305 g/cm^3 and M_w = 73.09 g/ mol) was supplied by DOP ORGANIK KIMYA, Turkey. 1-Methyl-2-Pyrrolidone (NMP) (> 99% C_5H_9NO, ρ = 1.028 g/cm^3 and M_w = 99.13 g/mol) was obtained from CHEM-LAB, Belgium. Commercial sea salt and distilled water were used in the MD experiments and all chemicals were used as received. Fig. 1 illustrates the chemical structure of PES and PVDF polymer.

2.2. Membrane dope and filler concentration

Pure PES and its composite with GNPs (PES/GNPs) as well as PES/PVDF blend and its composite with GNPs (PES/PVDF/GNPs) membranes were prepared and their characteristics were compared to our previously prepared pure PVDF and its composite with GNPs (PVDF/GNPs) [62]. The solvent mixture for the prepared membranes is DMF and NMP by 90:10 vol.%, respectively. The PES solution was prepared through dissolving 23 wt.% PES in the solvent mixture and stirring overnight at 80°C. To prepare the composite (PES/GNPs) membranes, modified graphene nanoplatelets were added first to the solvent mixture at five different weight ratios, namely 1, 2, 2.5, 3, and 4% of the used polymer content weight, respectively and the suspension was sonicated for 3 h. Then, PES was added and stirred overnight at 80°C. The effect of the content variation of the GNPs on the membrane hydrophobicity was determined by measuring the static water contact angle of the prepared membranes. The optimum filler ratio was chosen corresponding to the highest hydrophobic PES/GNPs membrane produced (i.e., the concentration at the highest static water contact angle). As for the PES/PVDF membrane dope, 17.25 wt.% PES and 5.75 wt.% PVDF (3:1 w/w) were added to the solvent mixture. For preparing the PES/PVDF/GNPs composite membrane, 2 wt.% of the GNPs was added to the solvent mixture and then the filler suspension was sonicated for 1 h. After that, 3:1 w/w% of PES flakes to PVDF pellets, respectively, were added to the sonicated GNPs and the polymer/filler solution was stirred overnight. Before the electro spinning process, the polymer dope was sonicated again for at least 1 h to ensure the good suspension. Lithium chloride (LiCl) was added to all the solutions at about 0.05 wt.% of the polymer to enhance the electro-spinning process. Table 1 lists the composition of the fabricated membranes.

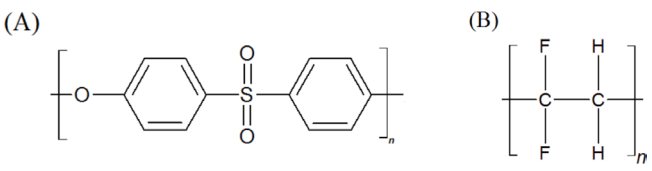

Fig. 1. Chemical structure of (A) poly (ethersulfone) (PES) and (B) polyvinylidene fluoride (PVDF).

2.3. Membranes fabrication

All the membranes were fabricated using an electro spinning system (NANON-3 MECC Co. Ltd., Japan). Fig. 2 illustrates a schematic diagram of the main components of the system. The electro spinning conditions used in this process are as follows: 22 kV applied voltage, a flow rate of 1.2 ml/h, and 13 cm vertical distance from the tip of the needle to the collector. The nanofibers were directly generated over a flat plate collector covered with aluminum foil and

Table 1
The composition of the fabricated membranes

Membrane	PES (wt. %)	PVDF (wt. %)	Graphene (wt. %)
Pure PES	23	–	–
PES + Graphene (1)	23	–	1
PES + Graphene (2)	23	–	2
PES + Graphene (3)	23	–	2.5
PES + Graphene (4)	23	–	3
PES + Graphene (5)	23	–	4
PES + PVDF	17.25	5.75	–
PES + PVDF + Graphene	17.25	5.75	2
Pure PVDF	–	14	–
PVDF + Graphene	–	14	2

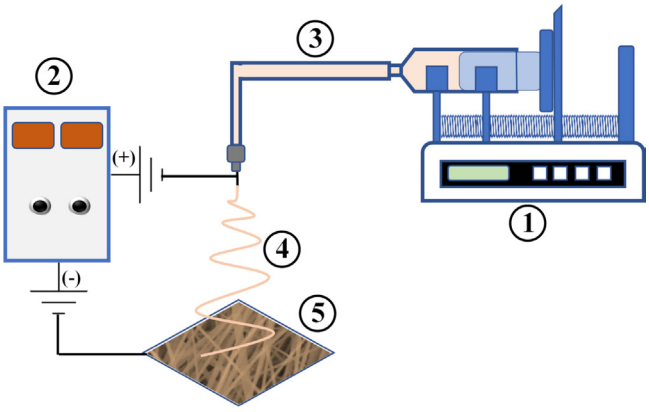

Fig. 2. Schematic diagram of main components of the electro spinning system: (1) Syringe pump, (2) high voltage power supply, (3) solution, (4) nanofibers and (5) slat plate collector.

topped by the support. During the entire process, the inner chamber was maintained at 40–50% humidity and 30°C temperature. These conditions were kept almost constant for all the membranes. The Electro spinning process took about 6 h. After that, the electro-spun membranes were put in a drying oven at 60°C for 24 h to ensure the complete removal of any residual solvents.

2.4. Membrane characterization

2.4.1. Static water contact angle measurement

Static water contact angle of the fabricated membranes was measured using a drop shape Analyzer system (DSA100, KRÜSS) paired with an image analysis software. Membrane samples were placed and deionized water droplets of about 7 µL volume were dropped on different spots of the membrane surface. A high precision camera then captured the droplet images at consecutive time frames and the right and left contact angles were estimated using the image analysis software. At least, three different readings were performed for two samples of each membrane to ensure precision and the average contact angle values were calculated and recorded.

2.4.2. Liquid entry pressure (LEP) determination

Liquid entry pressure (LEP; measures the minimum pressure at which liquid water can penetrate the membrane) for all the fabricated membranes was done using a simple configuration prepared in our lab. This configuration consists of a nitrogen gas cylinder, a small water tank, the membrane test cell, and a pressure gauge. First, a dry membrane sample was fitted inside the membrane cell. Then, the water tank was filled with distilled water and the nitrogen gas was slowly pumped to the water tank gradually raising the water static pressure and pushing it on the membrane surface. Then, the pressure was raised in small steps until bubbles started to form on the other side of the membrane. The pressure gauge reading at this point was considered the LEP. This simple experiment was repeated three times for each membrane and the results were averaged and recorded.

2.4.3. Scanning electron microscopy imaging

The surface morphology of the produced membranes was investigated using a scanning electron microscope (SEM, JEOL JCM-6000 plus, Japan). The membrane samples were coated with platinum before imaging. The SEM imaging was performed at an accelerating voltage of 15 kV. Several images at different magnification values were acquired at various sections for all the prepared samples. Image analysis was utilized for different samples to estimate the average fiber diameter, fiber size and average pore size using Image J software (NIH) [63]. There are more accurate techniques to measure average pore size, like 'Mercury porosimetry'. However, due to the lack of appropriate equipment, Image J software was used like previous studies [64,65]. To increase the estimation accuracy as much as possible, more than 10 different SEM images were analyzed for each membrane and the average pore size value was recorded.

2.4.4. X-ray diffraction analysis (XRD)

X-ray diffraction analysis was performed using (XRD, Shimadzu Xlab 6100, Japan) for the fabricated membranes. Readings were recorded at a 2θ range from 10° to 80°.

2.4.5. Membrane thickness measurement

Thickness of the fabricated membranes was measured by using a digital micrometer (range: 0–25 mm, precision: 2 µm, HDT, China). Six readings of three different samples for each fabricated membrane were executed and their average value was calculated.

2.4.6. Membrane porosity determination

Membrane average porosity, which can be described as the ratio of the membrane pores volume to the total volume of the membrane [66] was calculated using a gravimetric method [67,68]. Three different samples of each membrane were first weighed after drying for 24 h at 60°C (W_d). Then, the membrane was immersed in an ethanol bath (purity >99%) for 10 minutes to ensure saturation with ethanol. After that, the samples were removed from the bath and immediately weighed again within 2 s from removal (W_{sat}). The sample porosity was determined using Eq. (1) [67–69]. Finally, the average porosity was calculated for all the membranes.

$$\varepsilon = \frac{\dfrac{\left(W_{sat} - W_d\right)}{\rho_{eth.}}}{\dfrac{\left(W_{sat} - W_d\right)}{\rho_{eth.}} + \dfrac{W_d}{\rho_{poly.}}} \tag{1}$$

where ε represents the porosity, W_{sat} is the saturated sample weight (g), W_d is the dry sample weight (g) and $\rho_{eth.}$ and $\rho_{poly.}$ are the densities of the ethanol and the polymer material (g/cm^3) respectively. Three different samples were used for each membrane and the average value was calculated.

2.5. Membrane performance using direct contact membrane distillation (DCMD)

The produced membranes were tested using a MD cell, which was fabricated at the workshop of Egypt-Japan University of Science and Technology (E-JUST). Fig. 3 shows a schematic diagram of the test cell assembly which incorporates an effective membrane surface area of about 19.89 cm^2 with feed and permeate channels dimensions of (45 × 45 × 3 mm). Rubber gaskets (around 1.5 mm × 1.5 mm^2 size) are used at the sides of the membrane to prevent water leakage and act as membrane supporters.

Fig. 4 illustrates a schematic diagram and a pictorial view of the actual test rig used in this work. Three different sets of experiments were carried out to investigate the effect of several feed inlet conditions on the performance of the fabricated membranes. Counter current flow arrangement was chosen for all the experiments to improve the heat transfer. During the experiments, a water bath (Cole-Parmer, USA) was used to control the feed inlet temperature ($T_{f,\,in}$), while a cooling setup (Alpha RA 8, LAUDA) con-

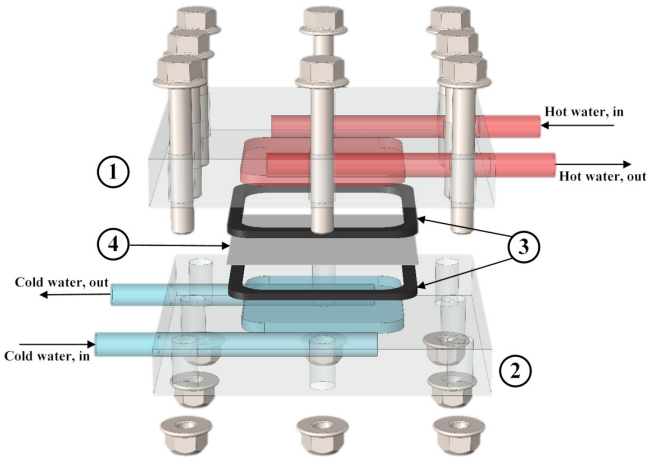

Fig. 3. Schematic diagram for the membrane distillation (MD) cell components. (1) feed channel, (2) permeate channel, (3) gaskets, and (4) the tested membrane.

trolled the permeate inlet temperature ($T_{per,\ in}$). A micro pump (Cole-Parmer, USA) was used to control and monitor the feed inlet flow rate and a micro gear pump (WT3000-1JB, LONGER) was used for the permeate side. Throughout the experiments, the inlet and outlet temperatures of the feed and permeate channels were measured by four type-k thermocouples (model: TSK, JUST CO., LTD., Japan) and recorded via a multi-channel data logger (midi LOGGER GL840, GRAPHTEC, Japan). Feed inlet pressure was measured using a digital double pressure meter (HND-P Series, KOBOLD Instruments Inc, USA). Total dissolved salts (TDS) of the feed and permeate sides were measured before and after each experiment using Waterproof CON 150 Meter (Eutech Instruments Pte Ltd).

2.5.1. Effect of the feed inlet temperature

The effect of the feed inlet temperature ($T_{f,in}$) on the performance of the fabricated membranes was studied. The

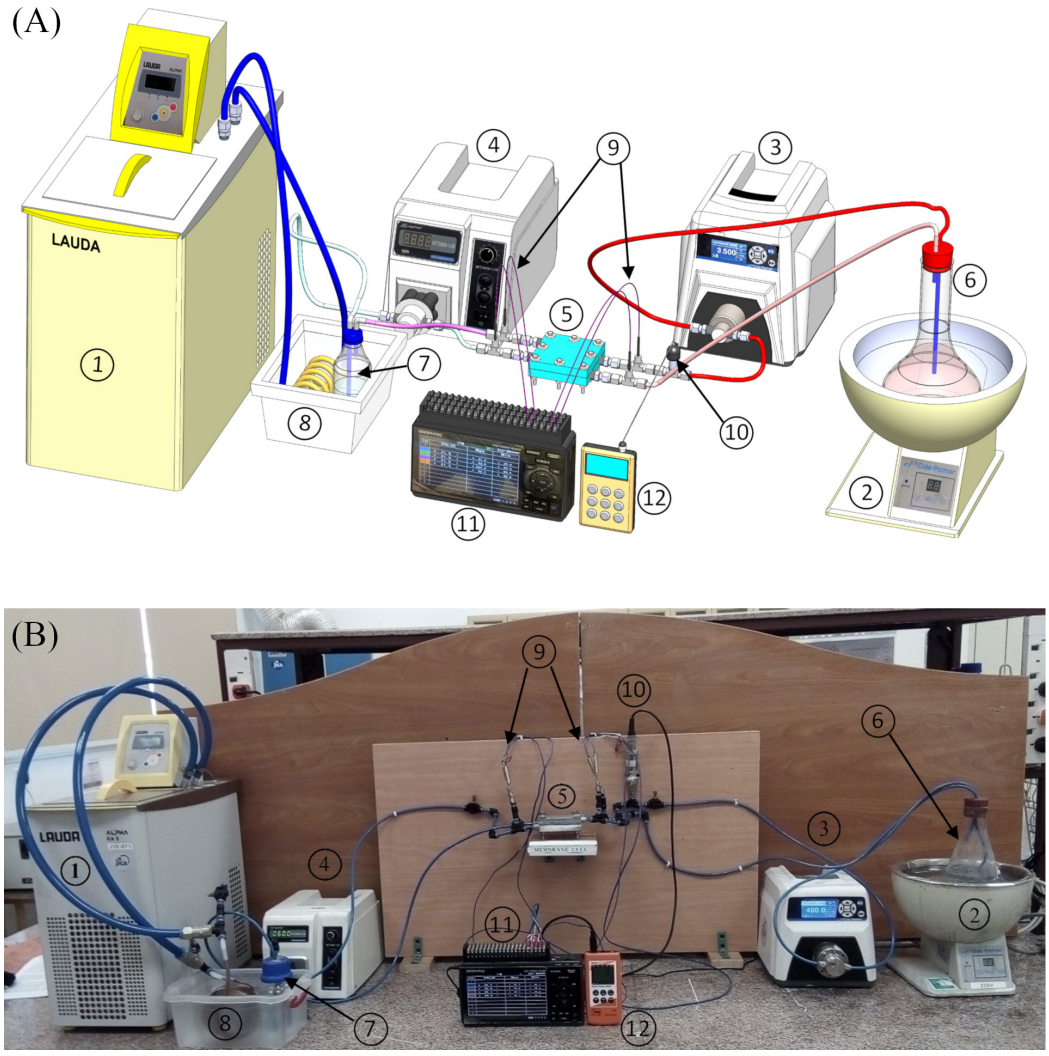

Fig. 4. (A) Schematic diagram and (B) Pictorial view of the DCMD test rig: (1) chiller, (2) heater, (3) feed water pump, (4) permeate water pump, (5) membrane cell, (6) feed water bottle, (7) permeate water bottle, (9) thermocouples, (10) pressure transducer, (11) data logger, and (12) pressure logger.

inlet temperature of the feed saline water was changed from 35 to 65°C at 10°C increments, while the feed inlet flow rate was maintained at 18 l/h and the feed inlet salt concentration was kept at about 10000 ppm. The permeate inlet conditions were kept at 25°C temperature and 5 l/h flow rate throughout the experiments. The experimentation time for each membrane was about 12 h.

2.5.2. Effect of the feed inlet flow rate

The effect of the feed saline water inlet flow rate on the performance of the fabricated membranes was studied. The flow rate was raised from 12 to 30 l/h at 6 l/h increments. Meanwhile, the feed inlet temperature was maintained at 65°C and the feed inlet salt concentration was 10000 ppm. During all the experiments, the permeate inlet temperature was kept at 25°C temperature and permeate flow rate was kept at 5 l/h. This procedure lasted about 12 h/membrane.

2.5.3. Effect of the feed inlet salt concentration

The effect of the feed inlet salt concentration on the membranes' MD performance was investigated by changing it from around 3–5 ppm (distillate water) up to 30000 ppm at 10000 ppm steps. The feed saline water inlet temperature was 65°C and the feed saline water inlet flow rate was 30 l/h. The permeate inlet remained at 25°C temperature and 5 l/h flow rate throughout the experiments. The experiment time/membrane was about 12 h.

2.5.4. Membrane flux and salt rejection

To calculate the permeate flux, a precise balance was used to measure the mass of the permeate water bottle before and after each experiment. The difference in weight represented the total mass of the permeate. The permeate flux was then calculated using Eq. (2):

$$flux = \frac{m_{p2} - m_{p1}}{A * t} \tag{2}$$

where the permeate flux unit is kg/m²·h, m_{p2} is the permeate bottle mass after the experiment (kg), m_{p1} is the permeate bottle mass before the experiment (kg), A is the membrane effective area (m²), and t is the permeate collecting time (h).

To calculate the salt rejection ratio, waterproof CON 150 Meter (Eutech Instruments Pte Ltd), was used to measure the salt concentration (TDS) of the feed channel and in the permeate bottle before and after each experiment. Then the salt rejection ratio was calculated according to Eq. (3):

$$salt\ rejection = 1 - \frac{\left(\frac{m_{p2}c_{p2} - m_{p1}c_{p1}}{m_{p2} - m_{p1}}\right)}{C_f} \tag{3}$$

where c_{p2} is the permeate bottle salt concentration after the experiment (ppm), c_{p1} is the permeate bottle salt concentration before the experiment (ppm), and C_f is the feed inlet salt concentration (ppm).

3. Mathematical modeling

The total mass flux (J) [kg/(m²·s)] across the membrane area can be calculated using Eq. (4):

$$J = C\,\Delta P_v \tag{4}$$

where ΔP_v is the water vapor pressure difference [Pa] between the membrane sides which is the driving force for the vapor flux and C is the membrane mass transfer coefficient [kg m^{-2} s^{-1} Pa^{-1}]. P_v on either of the membrane sides may be estimated with Antoine equation [70]:

$$P_v = x_w\left(1 - 0.5x_{salt} - 10x_{salt}^{\,2}\right)\exp\left(23.1964 - \frac{3816.44}{T_m - 46.13}\right) \tag{5}$$

where x_w and x_{salt} are the water and salt mole fractions in the aqueous solution and T_m represents the average membrane surface temperature [K].

Because in DCMD the water is in direct contact with the membrane from both sides under atmospheric pressure, the viscous flow may be considered negligible [71]. The mass flux through the membrane pores may be controlled via three different diffusion mechanisms [72]; namely the ordinary molecular diffusion through the air gaps within the membrane pores, Knudsen diffusion through the membrane pores, or Poiseuille flow in the transitional area, which combines both previous mechanisms [73]. This is determined via Knudsen number (K_n) that is the ratio between the mean free path (λ) and the average pore size. The mean free path can be calculated for water using Eq. (6) [74]:

$$\lambda = \frac{k_B T_m}{9.86 * 10^{-20} * \pi p} \tag{6}$$

where k_B is the Boltzmann constant, p is the mean pressure in the membrane pores (for DCMD, is about 1 atm) and T_m is the mean temperature inside the membrane pores.

In the regions where $K_n < 0.01$, Molecular diffusion prevails, whilst when $K_n > 1$, Knudsen flow is dominant. However, in the transitional regions ($0.01 < K_n < 1$), vapor transport occurs due to effects from both diffusion mechanisms, and assuming a uniform pore size distribution, the mass transfer coefficient C may be estimated using Eq. (7) [75]:

$$C = \frac{\varepsilon}{\tau\delta}\left(\frac{3}{2r}\sqrt{\frac{\pi}{8}\frac{RT_m}{M}} + \frac{P_a RT_m}{MPD}\right)^{-1} \tag{7}$$

where ε, τ, δ, and r are the membrane porosity, tortuosity, thickness [m], and average pore radius [m], respectively. R is the universal gas constant [8.314 J/ (mole. K)], M is the molecular weight of water [0.018 kg/mol], P_a is the air partial pressure within the pores [Pa], P is the total pressure [Pa] and D is the water diffusion coefficient [m²/s].

Membranes porosity (ε), thickness (δ), and average pore radius (r), can be estimated through experimental measurements, while the membrane tortuosity (τ) can be estimated using Eq. (8) [76]:

$$\tau = \frac{(2-\varepsilon)^2}{\varepsilon} \tag{8}$$

The multiplication value PD is a function of T_m and can be calculated using the following relation:

$$PD = 1.895 * 10^{-5} * T_m^{2.072} \quad (9)$$

As can be seen from the previous relations, to be able to accurately estimate the value of the membranes mass transfer coefficients; *C*, we have to know the membrane surface temperatures at the feed ($T_{f,m}$) and at the permeate ($T_{p,m}$) sides. The problem with that is wheras we can measure the bulk temperature at both sides ($T_{f,b}$, $T_{p,b}$), we cannot do the same for the membrane surface temperatures. To do that, we have to perform some iterations.

The total heat flux through the membrane; *Q* [W/m^2], consists mainly of evaporation heat transfer and conduction heat transfer within the membrane matrix and can be calculated using Eq. (10):

$$Q = h_f\left(T_{f,b} - T_{f,m}\right) = J * DH_v + \frac{k_m}{d}\left(T_{f,m} - T_{p,m}\right) = h_p\left(T_{p,m} - T_{p,b}\right) \quad (10)$$

where h_f, h_p are the convective heat transfer coefficients in the feed and permeate sides [W/m^2·K], ΔH_v is the latent heat of evaporation [kJ/kg] and k_m represents the membrane thermal conductivity [W/m·K].

h_f and h_p can be estimated from Nusselt number (Nu) that can be calculated at the feed and permeate sides using the following relation for laminar flow [3]:

$$Nu = 4.36 + \frac{0.036\,\mathrm{Re}\,\mathrm{Pr}\left(\frac{D}{L}\right)}{1 + 0.0011\,\mathrm{Re}\,\mathrm{Pr}\left(\frac{D}{L}\right)^{0.8}} \quad (11)$$

where Re, *Pr* are Reynolds and Prandtl numbers, respectively. *D* is the hydraulic diameter of the channel [m] and *L* is the channel length [m].

The latent heat of evaporation; ΔH_v, can be calculated as a function of T_m with Eq. (12):

$$\Delta H_v = 1.7535 T_m + 2024.3 \quad (12)$$

And k_m can be estimated using Eq. (13):

$$k_m = \left(\frac{\varepsilon}{k_g} + \frac{1-\varepsilon}{k_s}\right)^{-1} \quad (13)$$

where k_g and k_s are the gas thermal conductivity and the polymer thermal conductivity, respectively [77].

Eq. (10) can be simplified to get $T_{f,m}$ and $T_{p,m}$ as follows:

$$T_{f,m} = \frac{\frac{k_m}{d}\left(\frac{h_f}{h_p}T_{f,b} + T_{p,b}\right) - J\,DH_v + h_f T_{f,b}}{h_f + \frac{k_m}{d}\left(1 + \frac{h_f}{h_p}\right)} \quad (14)$$

and

$$T_{p,m} = \frac{\frac{k_m}{\delta}\left(\frac{h_p}{h_f}T_{p,b} + T_{f,b}\right) + J\,\Delta H_v + h_p T_{p,b}}{h_p + \frac{k_m}{\delta}\left(1 + \frac{h_p}{h_f}\right)} \quad (15)$$

To accurately calculate the mass transfer coefficient, an algorithm is established, where T_m is assumed and the other variables are calculated using Eqns. (8)–(13). Then $T_{f,m}$ and $T_{p,m}$ are estimated and then T_m is recalculated until the relative error between the two consecutive values is less than 0.01%.

4. Results and discussion

4.1. Filler concentration

Fig. 5 illustrates the effect of adding different ratios of GNPs on the static water contact angle of the PES membranes as obtained via the drop shape Analyzer. As can be clearly seen from the figure, the static water contact angle was enhanced with the incorporation of GNPs from about 92° for pure PES membrane up to about 122.9° at 2 wt. % GNPs content. This is cannot be only accredited to the hydrophobicity of the GNPs because as seen from SEM images (see the following section), the filler is mostly enclosed inside the polymer fibers. Only a little amount of the filler was noticed on the fiber walls. The effect of increasing the membrane/fiber roughness as noticed from projections may be effective in increasing the static water contact angle in the membrane. However, a slight decrease in the measured static water contact angle was noticed at GNPs content higher than 2.5 wt. %. This phenomenon could be attributed to aggregation of the GNPs in the membrane matrix [78], which led to bad distribution of the GNPs and creation of several beads inside the membrane matrix as shown in the SEM images (Fig. 6) for 3 wt. % and 4 wt.% GNPs content. Meanwhile, the improvement in the static water contact angle when increasing the GNPs content from 2 to 2.5 wt.% is negligible (from 122.9 to 123.7°). For that, 2 wt. % GNPs ratio was chosen to complete this work.

4.2. Membrane characterization

The thickness and the porosity of the fabricated membranes are shown in Table 2. As noticed, the presence of the GNPs in the membrane matrix slightly decreased the membrane thickness (about 4.7% for the PES, 1.9% for the PVDF, and 4.2% for the PES/PVDF blend membrane). This may

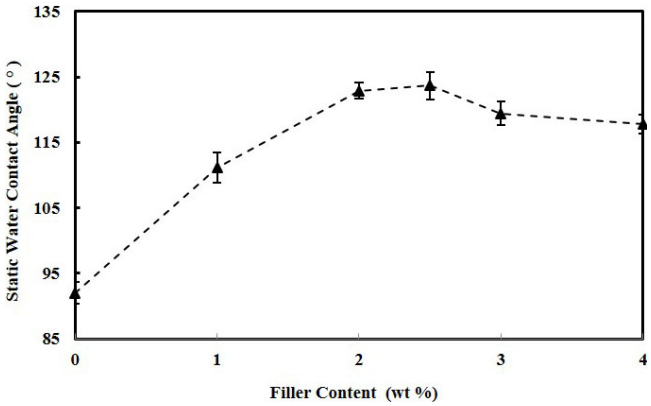

Fig. 5. Effect of filler content (%) on the static water contact angles on PES/GNPs composite membranes.

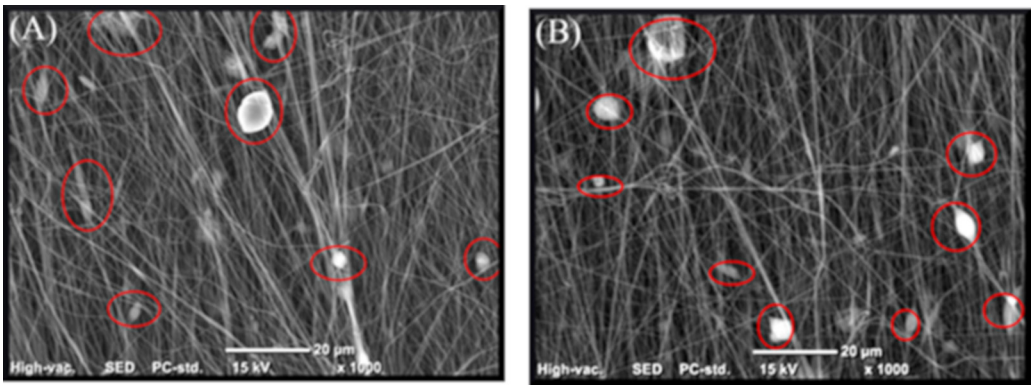

Fig. 6. SEM images of PES/GNPs composite membranes; (A) 3 wt. % and (B) 4 wt.% GNPs filler.

Table 2
Characteristics of the fabricated membranes (average fiber diameter, average pore size, membrane thickness, membrane porosity, static water contact angle, and liquid enter pressure (LEP)

Membrane	Average fiber diameter (µm)	Average pore size (µm)	Membrane thickness (µm)	Membrane porosity(%)	Static water contact angle (°)	LEP (kPa)
Pure PES	0.342 ± 0.06	0.455 ± 0.08	112 ± 2.1	92 ± 1.6	92 ± 1.7	NA
PES / GNPs	0.337 ± 0.04	0.423 ± 0.05	107 ± 2.4	89 ± 1.7	122.9 ± 1.2	NA
Pure PVDF	0.374 ± 0.06	0.494 ± 0.04	162 ± 2.5	92 ± 2.1	131.6 ± 2.3	85
PVDF / GNPs	0.352 ± 0.08	0.451 ± 0.05	159 ± 3.1	90 ± 1.8	141.3 ± 1.2	95
PES / PVDF blend	0.387 ± 0.07	0.428 ± 0.07	148 ± 2.2	91 ± 1.4	121.6 ± 0.6	80
PES / PVDF / GNPs	0.356 ± 0.05	0.379 ± 0.09	142 ± 1.8	88 ± 1.5	132.3 ± 0.8	85

*LEP is Water Liquid Entry Pressure – NA is Not Available due to being at a lower value than the detection limits.

be attributed to the enhancement of the attraction forces between the fibers during the electro spinning process due to an increase in the conductivity of the membrane dope that may increase the fiber layers attraction to each other, resulting in a more compact membrane.

The integration of GNPs in the membrane matrix resulted in slightly decreasing in the average fiber diameter for all fabricated membranes. The PES membrane average fiber diameter was reduced by about 1.5%, whereas the PVDF average fiber diameter was decreased by about 6.25%, and the PES/PVDF average fiber diameter also decreased by about 8.7% upon adding 2 wt.% GNPs filler. This small reduction in the fiber diameter may be also related to an increase in the electrical conductivity of the membrane dope with the GNPs addition, which may increase the solution polarity during electro spinning and improves the process, resulting in finer nanofibers.

Regarding the membrane porosity, all the fabricated membranes show high porosity (around 90%), which is a big advantage of the electro spinning technique over the other membrane fabrication techniques. This high porosity positively affects the membrane flux in the MD application. It can be also noticed that the porosity slightly decreased with the addition of the GNPs (around 3% reduction in the membrane porosity). In a similar trend, the average pore size was slightly decreased with adding the GNPs (around 8–11%). This also may be attributed to the enhancement in the solution conductivity after incorporating the GNPs, that led the fibers to move closer to each other, causing a decrease in the pore area, which is in agreement with previous researchers results [78].

The LEP values for the pure PES and PES/GNPs composite membranes could not be determined, as these membranes exhibited very low values of LEP that lower than the detection limits of the used gauge. Therefore, those membranes proved to be unsuitable for MD applications. However, with the addition of PVDF to the PES matrix by only 25%, the LEP increased dramatically to about 80 kPa. So, it can be used for MD applications. This reflects a significant improvement in the PES characteristics.

The uniformity and smoothness of the produced nanofibers as shown in the SEM images; Fig. 7, indicate an efficient electro spinning process. The absence of aggregation or big beads in the membranes with the GNPs filler indicate sufficient integration and good dispersion of the additive in the membrane matrix. The static water contact angle of the fabricated membranes in table 2 and Fig. 7, pure PES membrane exhibited the lowest static water contact angle with about 92°, whereas the PVDF/GNPs membrane displayed the highest static water contact angle with about 141°, which can be attributed to the natural hydrophobicity of the PVDF enhanced by the used hydrophobic GNPs filler. In all cases, the existence of the GNPs as a filler in the membrane matrix increased the contact angle noticeably. The static water contact angle of the PES/PVDF/GNPs composite membrane is around 132.3 ± 0.8°, which is very close to the static water contact angle of the pure PVDF membrane around 131.6 ± 2.3°. However, the PVDF/GNPs

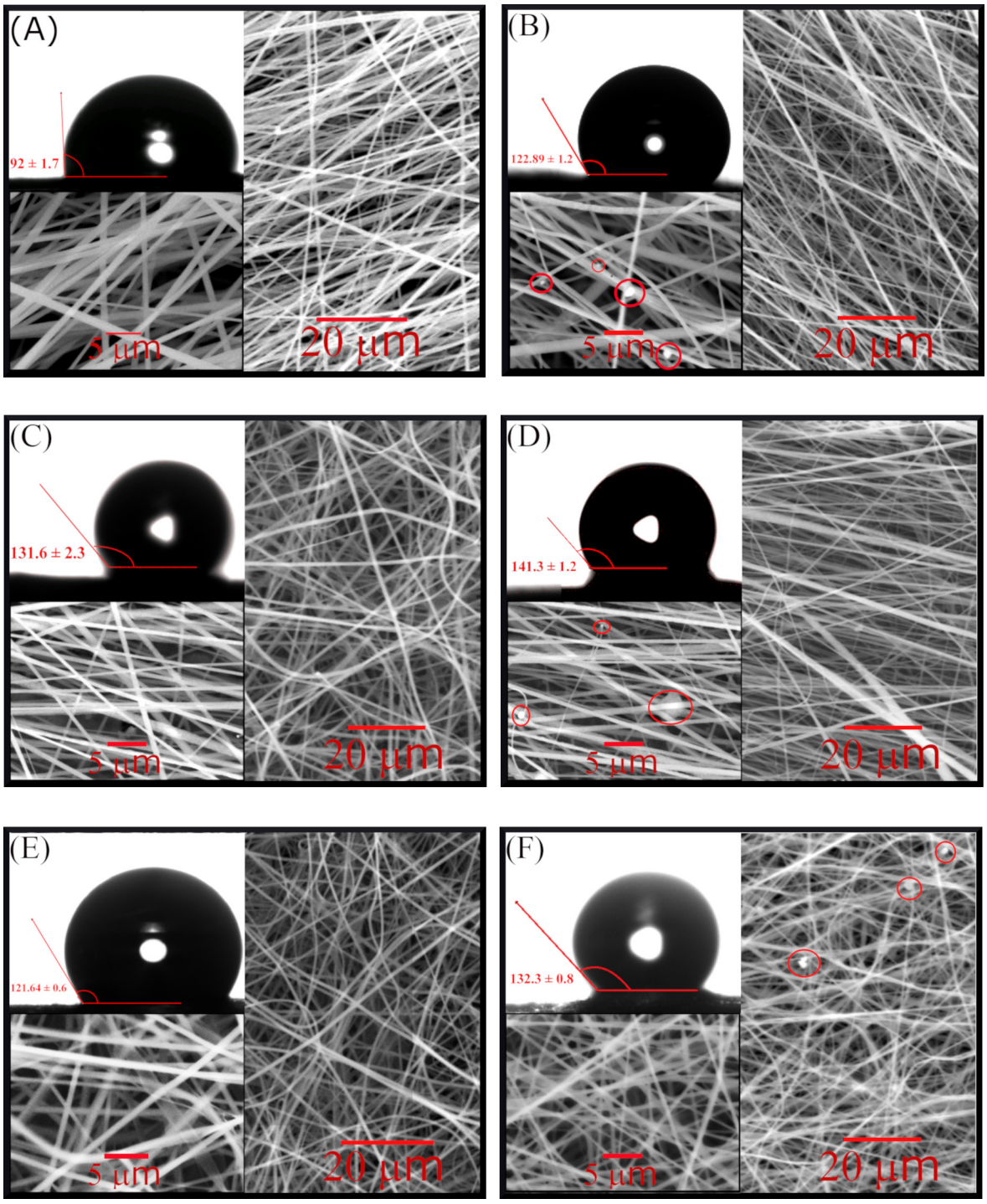

Fig. 7. SEM images and water contact angle for the produced membranes. (A) pure PES, (B) PES/GNPs, (C) pure PVDF, (D) PVDF/GNPs, (E) PES/PVDF blend, and (F) PES/PVDF/GNPs composite membrane.

has higher static water contact angle than both (pure PVDF and PES/PVDF/GNPs composite membranes). Indeed increasing the content of the PVDF than the 25% used in the PES/PVDF blend could increase the contact angle but at the expense of the membrane cost.

Fig. 8 shows the XRD pattern of pure and composite membranes as well as the used filler; GNPs. GNPs showed a strong peak at $2\theta = 26.3°$ followed by a peak at 54.7° that characterizes the existence of graphite [79]. These peaks appear as week peaks in all prepared composite membranes (PVDF/GNPs, PES/GNPs, and PES/PVDF/GNPs). This weakness can be related to the inclusion of the GNPs inside the polymer fiber as shown in the SEM images. The pure PVDF showed one obvious peak at $2\theta = 20.05°$ and

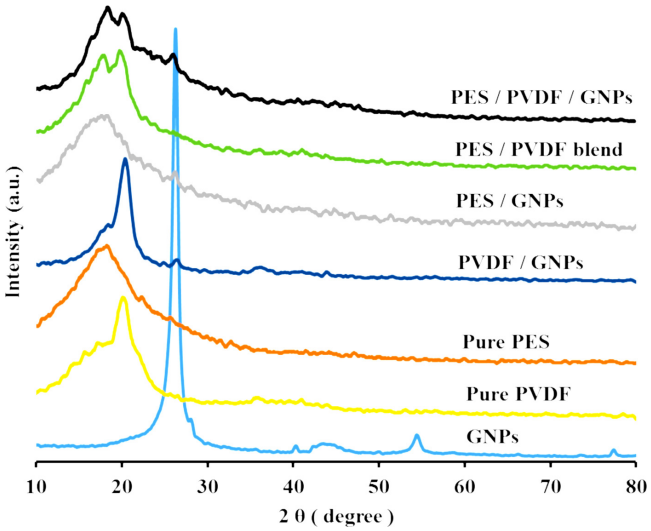

Fig. 8. XRD patterns of the fabricated membranes.

three weak peaks at 2θ = 18.4°, 26.4°, and 38.5°. The peaks at 2θ =18.4°, 20.05, 26.4° and 38.5° were related to (020), (100), (021) and (002) crystalline peaks of PVDF α crystalline phase, respectively [80]. The peak at 2θ = 20.05° can be shown in all other membranes incorporating PVDF. The pure PES membrane shows a broad peak around 2θ = 18.7° which characterizes PES and is shown in all other fabricated membranes included PES [81].The novel prepared PES/PVDF/GNPs membrane showed all of the above characteristic peaks that confirms the existence of GNPs and the other PES/PVDF blend polymers.

4.3. Membrane performance

Only four membranes were used for the performance evaluation test using a DCMD test rig, as the pure PES membrane and the PES/GNPs composite membranes proved to have a very low LEP to be used. The four membranes are pure PVDF, PVDF/GNPs composite, PES/PVDF blend, and PES/PVDF/GNPs composite membranes. They were all tested to investigate the effect of the feed saline water inlet temperature, the feed saline water flow rate, and salt concentration on their performance.

4.3.1. Effect of the feed saline water inlet temperature

The feed saline water inlet temperature was changed from 35 to 65°C at 10°C increments, while flow rate and salt concentration were maintained at 18 l/h and 10000 ppm, respectively. As shown in Fig. 9, increasing the feed saline water inlet temperature has a positive effect on the performance of the tested membranes, as it increases their productivity. This is due to increase the partial vapor pressure difference between the two sides, resulting in enhancing the driving force for the vapor flow through the membrane pores. As noticed, the membrane with the best performance was the PVDF/GNPs composite membrane. It reached a flux of 16.75 kg/m^2·h at 65°C and the worst membrane performance (11.6 kg/m^2·h) was for the PES/PVDF blend membrane. However, the PES/PVDF/GNPs

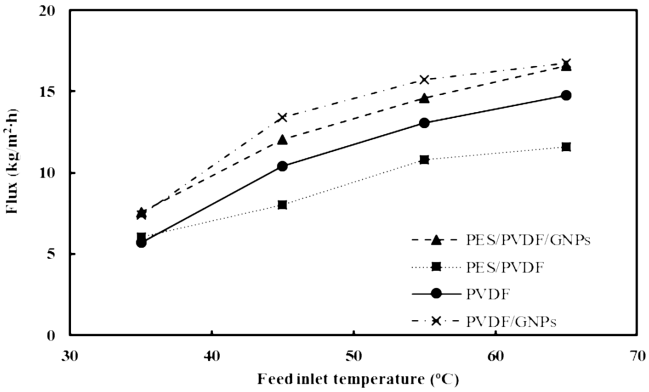

Fig. 9. Effect of feed saline water inlet temperature on the performance of the fabricated membranes.

composite membrane achieved very close flux values to the best membrane with 16.6 kg/m^2·h at the same conditions. So, adding 2 wt.% GNPs filler increased the flux of the PES/PVDF blend membrane by 43% to be comparable to the costly PVDF/GNPs composite membrane. This may be because adding graphene to the membrane resulted in multi-level membrane surface roughness, which increased its hydrophobicity. It also increased the LEP. The GNPs large aspect ratio also composed Nano and micro-scale lumps over the surface which helped to stop the water molecules penetration into the membrane pores and permitted more vapor to pass through due to the high porosity of the electro-spun membranes. GNPs also formed diffusion paths for the flux via continuous adsorption/desorption processes. This all resulted in higher vapor flux. This agrees with previous results [82].

4.3.2. Effect of the feed saline water flow rate

Fig. 10 displays the relationship between the feed saline water flow rate and the permeate flux. The feed flow rate increased from 12 to 30 l/h at 6 l/h increments, while the feed temperature and salt concentration were maintained at 65°C and 10000 ppm, respectively. As noticed from Fig. 10, at low flow rates, the flux values are very close for all the fabricated membranes. This may be

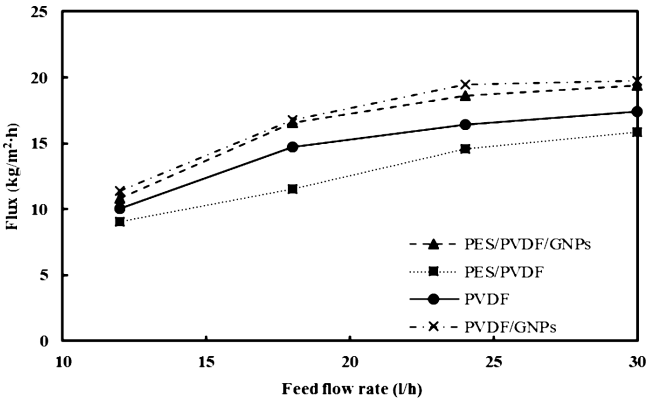

Fig. 10. Effect of the feed saline water inlet flow rate on the performance of the fabricated membranes.

related to the fact that the boundary layer effects are dominant. Increasing the feed flow rate enhanced the permeate flux for all the membranes. This is due to higher heat transfer coefficient which leads to less temperature polarization between the membrane surface and the bulk temperature that enhancing the vapor driving force through the membrane pores. However, at higher flow rates, the flux enhancement slowed down. This may be attributed to an increase in the conduction heat loss across the membranes, which hindered flux enhancement. This is similar in trend to previously reported researches [83]. Also, it is noticed that the performance of the PES/PVDF/GNPs composite membrane is very close to the membrane with the best performance (PVDF/GNPs; 19.77 kg/m²·h). It reached a flux value of 19.35 kg/m²·h at 30 l/h, which is only about 2.1% (within the error limits) lower than the flux of PVDF/GNPs membrane. It can also be noticed that adding the GNPs filler increased the flux by a ratio up to 22.5% in case of the PES/PVDF blend membrane (15.8 kg/m²·h) and up to 11.2% for the pure PVDF membrane (17.4 kg/m²·h).

4.3.3. Effect of feed inlet salt concentration

Fig. 11 illustrates the effect of changing feed inlet salt concentration on the membranes flux. The feed inlet salt concentration was changed from distillate water (3:5 ppm) up to 30000 ppm at 10000 ppm steps, while temperature and flow rate were kept at 65°C and 30 l/h, respectively. As can be seen from Fig. 11, at relatively low concentrations, the permeate flux is high, which suggests low concentration polarization in the membrane feed boundary. This minimizes the effects of salt precipitation on the permeate flux which agrees with other researchers [84,85]. However, increasing the feed inlet salt concentration significantly decreases the permeate flux. This may be related to the drop of the water vapor pressure at higher salt concentrations at the same working temperatures. This drop was caused by the decrease in the water activity in the feed flow. This caused a growth in the salt concentration over the membrane surface, which led to increase the precipitation of the salt over the membrane surface. As seen in Fig. 12, SEM images of the PES/PVDF/GNPs composite membrane after being exposed to a high salt concentration of 30000 ppm for about 12 h. The images show that salt particles formed a layer over the membrane surface. This layer hindered vapor flow through the membrane and decreased the membrane surface temperature. This effect reduced the flux of all the membranes as follows: Pure PVDF; 52.4%, PVDF/GNPs; 45.4%, PES/PVDF blend; 62.3%, and PES/PVDF/GNPs; 47%. It may also lead to a membrane failure or salt penetration through the membrane pores if not treated properly.

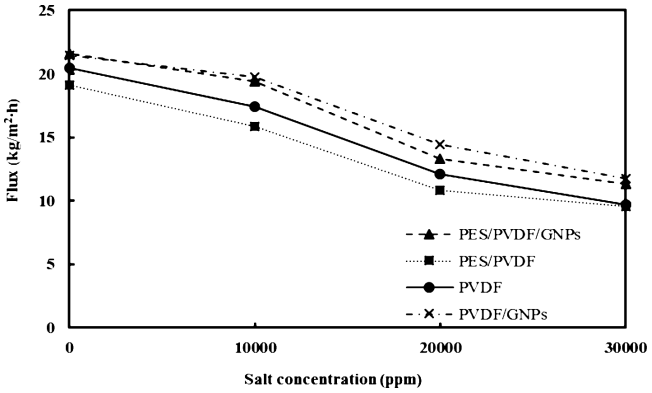

Fig. 11. Effect of feed inlet salt concentration on the performance of the fabricated membranes.

4.4. Mathematical modeling

As a case study, the flow rate results were chosen for mass transfer coefficient analysis.

First, Knudsen number (K_n) was calculated for each membrane to recognize the transfer mechanism. Table 3 shows the calculated values assuming that T_m is the average of the bulk temperatures (318 K).

As shown in Table 3, K_n for all fabricated membranes is between 0.01 and 1. Then, the flow mechanism is transitional that combines Knudsen flow and normal diffusion.

Then, an algorithm was used as previously explained in the mathematical modeling section, to predict the values of the mass transfer coefficients for the different membranes. The values of the mass transfer coefficients at different flow rates are shown in Fig. 13.

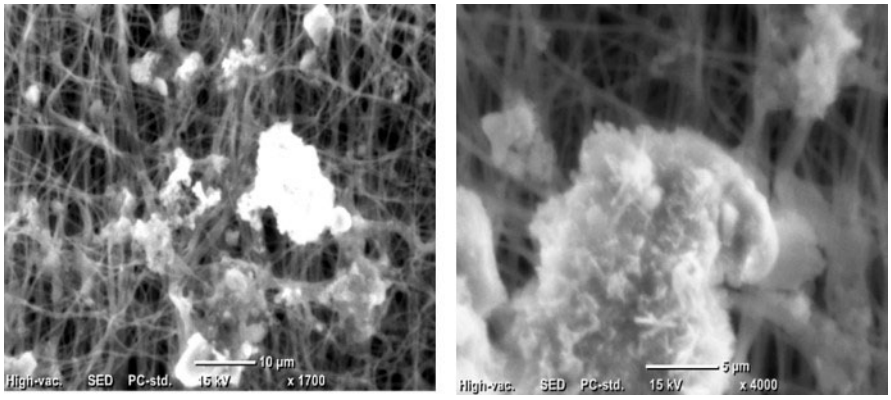

Fig. 12. SEM images of salt precipitation over the PES/PVDF/GNPs composite membrane surface; (A) ×1700 and (B) ×4000 magnification

Table 3
Calculated Knudsen number for the different fabricated membranes

Membrane	Average pore size (μm)	Mean free path (λ) (μm)	Knudsen number (Kn)
Pure PVDF	0.494 ± 0.04	0.14	0.283
PVDF / GNPs	0.451 ± 0.05	0.14	0.310
PES / PVDF blend	0.428 ± 0.07	0.14	0.327
PES / PVDF / GNPs	0.379 ± 0.09	0.14	0.369

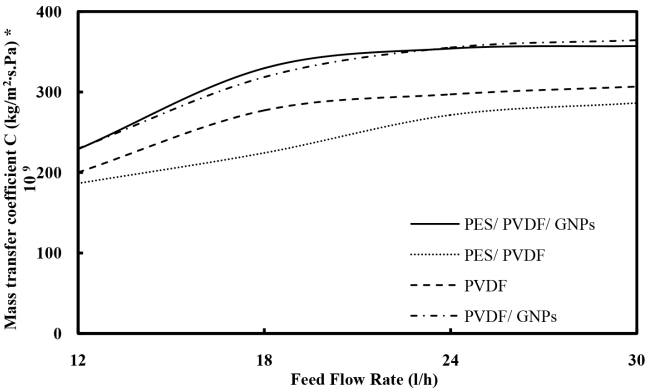

Fig. 13. Calculated mass transfer coefficient for the fabricated membranes at different feed flow rates.

Table 4
Average mass transfer coefficients for the different membranes

Membrane	Average mass transfer coefficient (C) [kg/m²·s·Pa] * 10^9
Pure PVDF	270.313
PVDF/GNPs	317.05
PES/PVDF blend	242.157
PES/PVDF/GNPs	317.42

As can be seen from Fig. 13, the mass transfer coefficient tends to slightly increase with the feed flow rate, as it provides better heat transfer and higher driving force. The average mass transfer coefficients within the studied range are tabulated in Table 4. As noticed, the PES/PVDF/GNPs membrane has the highest average mass transfer coefficient, even higher than average mass transfer coefficient of the PVDF/GNPs membrane. This is may be due to the high porosity of the PES membrane.

5. Conclusions

Pure PES, pure PVDF, PES/GNPs, PVDF/GNPs, PES/PVDF blend and PES/PVDF/GNPs composite membranes were fabricated and were characterized and evaluated for desalination by using MD process. The optimal ratio of the GNPs filler was found to be about 2 wt.%. Two of the membranes (pure PES and PES/GNPs composite) proved to be unsuitable for MD applications, as their LEP was very low (under the detection limits). The PVDF/GNPs composite membrane shows the best performance membrane; the best performance at change the feed inlet conditions. However, the novel PES/PVDF/GNPs composite membrane has favorable qualities and high performance comparable to the high cost pure PVDF and PVDF/GNPs composite membranes. As general trend, replacement 75% of the PVDF content by PES polymer resulted in reduction in the performance of produced PES/PVDF blend membrane compared to the performance of both pure PVDF and PVDF/GNPs composite membranes. Whereas, only 2 wt.% GNPs included in the blend to form PES/PVSF/GNPs composite resulted in a significant performance to be comparable to the costly best performance PVDF/GNPs composite membrane. The PES/PVSF/GNPs composite membrane exhibited high hydrophobicity with static water contact angle of about 132.3°. In the DCMD tests, it achieved a flux of 19.35 kg/m²·h at feed inlet temperature of 65°C, flow rate of 30 l/h, and salt concentration of 10000 ppm, which is only 2.1% lower than the flux of the PVDF/GNPs composite membrane at the same conditions. Also, the PES/PVDF/GNPs membrane has the highest calculated average mass transfer coefficient, which is even slightly higher than average mass transfer coefficient of the PVDF/GNPs membrane. These favorable characteristics, paired with the fact that we used commercial PES, which is much cheaper than the cost of PVDF, results in a cost reduction of about 50–75% compared to the PVDF/GNPs composite membrane. This composite membrane shows a good potential to be used instead of other conventional membranes in MD applications.

6. Recommendations and future work

Although, the produced membrane showed a potential for MD applications, there is still much room for improvement. The salt precipitation problem at high feed inlet concentrations should be addressed either by changing the membrane cell design or by other additives [86]. The long-term performance of the membrane also should be investigated, as it presents an important factor for practical implementation. Cell design optimization to produce higher thermal efficiency, should also be addressed. The effect of adding micro-feed channels may reduce temperature polarization should also be considered. A deeper mathematical model to accurately predict the flux at different conditions will be considered as a following step.

Acknowledgment

The authors wish to acknowledge the financial support of Egypt-Japan University of Science and Technology and the Egyptian Ministry of higher education.

Symbols

M_w	—	Molecular weight (g/mol)
W_d	—	Dry sample weight (g)
W_{sat}	—	Saturated sample weight (g)
ε	—	Porosity
ρ	—	Density (g/cm^3)
ρ_{eth}	—	Density of ethanol (g/cm^3)
ρ_{pol}	—	Density of polymer material (g/cm^3)

References

[1] I.M. Mujtaba, The role of PSE community in meeting sustainable freshwater demand of tomorrow's world via desalination, Comput. Aided Chem. Eng., 31 (2012) 91–98.
[2] M.K. Souhaimi, T. Matsuura, Membrane distillation: Principles and Applications, Elsevier, 2011.
[3] A. Alkhudhiri, N. Darwish, N. Hilal, Membrane distillation: a comprehensive review, Desalination, 287 (2012) 2–18.
[4] E. Drioli, A. Ali, F. Macedonio, Membrane distillation: recent developments and perspectives, Desalination, 356 (2015) 56–84.
[5] P. Wang, T.-S. Chung, Recent advances in membrane distillation processes: Membrane development, configuration design and application exploring, J. Membr. Sci., 474 (2015) 39–56.
[6] D.-W. Cho, H. Song, K. Yoon, S. Kim, J. Han, J. Cho, Treatment of simulated coalbed methane produced water using direct contact membrane distillation, Water, 8 (2016) 194.
[7] M. Tomaszewska, Membrane distillation-examples of applications in technology and environmental protection, Pol. J. Environ. Stud., 9 (2000) 27–36.
[8] A. Ashraf, H. Salih, S. Nam, S.A. Dastgheib, Robust carbon nanotube membranes directly grown on Hastelloy substrates and their potential application for membrane distillation, Carbon, 106 (2016) 243–251.
[9] A.K. Fard, T. Rhadfi, M. Khraisheh, M.A. Atieh, M. Khraisheh, N. Hilal, Reducing flux decline and fouling of direct contact membrane distillation by utilizing thermal brine from MSF desalination plant, Desalination, 379 (2016) 172–181.
[10] M.E. Leitch, C. Li, O. Ikkala, M.S. Mauter, G.V. Lowry, Bacterial nanocellulose aerogel membranes: novel high-porosity materials for membrane distillation, Environ. Sci. Tech. Let., 3 (2016) 85–91.
[11] J. Phattaranawik, R. Jiraratananon, Direct contact membrane distillation: effect of mass transfer on heat transfer, J. Membr. Sci., 188 (2001) 137–143.
[12] A. Alkhudhiri, N. Hilal, Air gap membrane distillation: a detailed study of high saline solution, Desalination, 403 (2017) 179–186.
[13] A.E. Khalifa, Water and air gap membrane distillation for water desalination–an experimental comparative study, Sep. Purif. Technol., 141 (2015) 276–284.
[14] Y.C. Woo, L.D. Tijing, M.J. Park, M. Yao, J.-S. Choi, S. Lee, S.-H. Kim, K.-J. An, H.K. Shon, Electro spun dual-layer non-woven membrane for desalination by air gap membrane distillation, Desalination, 403 (2017) 187–198.
[15] L. Basini, G. D'Angelo, M. Gobbi, G. Sarti, C. Gostoli, A desalination process through sweeping gas membrane distillation, Desalination, 64 (1987) 245–257.
[16] M. Khayet, P. Godino, J.I. Mengual, Theory and experiments on sweeping gas membrane distillation, J. Membr. Sci., 165 (2000) 261–272.
[17] V. Perfilov, V. Fila, J.S. Marcano, A general predictive model for sweeping gas membrane distillation, Desalination, 443 (2018) 285–306.
[18] M.A.E.-R. Abu-Zeid, Y. Zhang, H. Dong, L. Zhang, H.-L. Chen, L. Hou, A comprehensive review of vacuum membrane distillation technique, Desalination, 356 (2015) 1–14.
[19] L. Li, K.K. Sirkar, Studies in vacuum membrane distillation with flat membranes, J. Membr. Sci., 523 (2017) 225–234.
[20] J. Zhang, M. Duke, M. Hoang, Z. Xie, A. Groth, C. Tun, S. Gray, Modelling of vacuum membrane distillation, J. Membr. Sci., 434 (2013) 1–9.
[21] M. El-Bourawi, Z. Ding, R. Ma, M. Khayet, A framework for better understanding membrane distillation separation process, J. Membr. Sci., 285 (2006) 4–29.
[22] L. Eykens, K. De Sitter, C. Dotremont, L. Pinoy, B. Van der Bruggen, Coating techniques for membrane distillation: An experimental assessment, Sep. Purif. Technol., 193 (2018) 38–48.
[23] Z. Xu, Z. Liu, P. Song, C. Xiao, Fabrication of super-hydrophobic polypropylene hollow fiber membrane and its application in membrane distillation, Desalination, 414 (2017) 10–17.
[24] S. Munirasu, F. Banat, A.A. Durrani, M.A. Haija, Intrinsically super hydrophobic PVDF membrane by phase inversion for membrane distillation, Desalination, 417 (2017) 77–86.
[25] H. Zhang, M. Liu, D. Sun, B. Li, P. Li, Evaluation of commercial PTFE membranes for desalination of brine water through vacuum membrane distillation, Chem. Eng. Process, 110 (2016) 52–63.
[26] Y. Yang, Q. Liu, H. Wang, F. Ding, G. Jin, C. Li, H. Meng, Super hydrophobic modification of ceramic membranes for vacuum membrane distillation, Chin. J. Chem. Eng., 25 (2017) 1395–1401.
[27] M.S. Fahmey, A.-H.M. El-Aassar, M.M. Abo-Elfadel, A.S. Orabi, R. Das, Comparative performance evaluations of nanomaterials mixed polysulfone: A scale-up approach through vacuum enhanced direct contact membrane distillation for water desalination, Desalination, (2017).
[28] S. Mansour, A. Giwa, S. Hasan, Novel graphene nanoplatelets-coated polyethylene membrane for the treatment of reject brine by pilot-scale direct contact membrane distillation: An optimization study, Desalination, 441 (2018) 9–20.
[29] J. Zuo, T.-S. Chung, Metal-organic frame work-functionalized alumina membranes for vacuum membrane distillation, Water, 8 (2016) 586.
[30] X. Wei, B. Zhao, X.-M. Li, Z. Wang, B.-Q. He, T. He, B. Jiang, CF4 plasma surface modification of asymmetric hydrophilic polyethersulfone membranes for direct contact membrane distillation, J. Membr. Sci., 407 (2012) 164–175.
[31] M.R. Elmarghany, A.H. El-Shazly, M.S. Salem, M.N. Sabry, N. Nady, Thermal analysis evaluation of direct contact membrane distillation system, Case Stud. Therm. Eng., 13 (2019) 100377.
[32] E.C. Mapunda, B.B. Mamba, T.A. Msagati, Carbon nanotube embedded PVDF membranes: Effect of solvent composition on the structural morphology for membrane distillation, Phys. Chem. Earth., Parts A/B/C, 100 (2017) 135–142.
[33] H. Abdallah, A. Moustafa, A.A. AlAnezi, H. El-Sayed, Performance of a newly developed titanium oxide nanotubes/polyethersulfone blend membrane for water desalination using vacuum membrane distillation, Desalination, 346 (2014) 30–36.
[34] M.R. El-Marghany, A.H. El-Shazly, M.S.A. Salem, M.N. Sabry, N. Nady, Novel membrane suitable for membrane distillation: effect of mixed nanofillers on the membrane performance, Key Eng. Mater., 801 (2019) 325–330.
[35] A. Jafari, M.R.S. Kebria, A. Rahimpour, G. Bakeri, Graphene quantum dots modified polyvinylidenefluride (PVDF) nanofibrous membranes with enhanced performance for air Gap membrane distillation, Chem. Eng. Process., 126 (2018) 222–231.
[36] M. Khayet, M. García-Payo, L. García-Fernández, J.J.D. Contreras-Martínez, Dual-layered electro spun nanofibrous membranes for membrane distillation, Desalination, 426 (2018) 174–184.
[37] C. Su, C. Lu, H. Cao, K. Tang, J. Chang, F. Duan, X. Ma, Y. Li, Fabrication and post-treatment of nanofibers-covered hollow fiber membranes for membrane distillation, J. Membr. Sci., 562 (2018) 38–46.
[38] A.C. Chinyerenwa, H. Wang, Q. Zhang, Y. Zhuang, K.H. Munna, C. Ying, H. Yang, W. Xu, Structure and thermal properties of porous polylactic acid membranes prepared via phase inversion induced by hot water droplets, Polymer, 141 (2018) 62–69.

[39] S. Ichikawa, T. Kawai, Fractionation of binary polymer blend based on size distribution of particles prepared by phase inversion method, Polymer, 125 (2017) 276–282.
[40] N. Agoudjil, S. Kermadi, A. Larbot, Synthesis of inorganic membrane by sol–gel process, Desalination, 223 (2008) 417–424.
[41] J.P.C. Fernandes, V.H. Mareau, L. Gonon, Co-localized AFM-Raman: A powerful tool to optimize the sol-gel chemistry of hybrid polymer membranes for fuel cell, Polymer, 137 (2018) 231–244.
[42] Y. Yang, P. Wang, Preparation and characterizations of a new PS/TiO_2 hybrid membranes by sol–gel process, Polymer, 47 (2006) 2683–2688.
[43] C. Feng, K. Khulbe, T. Matsuura, S. Tabe, A. Ismail, Preparation and characterization of electro-spun nanofiber membranes and their possible applications in water treatment, Sep. Purif. Technol., 102 (2013) 118–135.
[44] L. Francis, H. Maab, A. AlSaadi, S. Nunes, N. Ghaffour, G.L. Amy, Fabrication of electro spun nanofibrous membranes for membrane distillation application, Desal. Water Treat., 51 (2013) 1337–1343.
[45] L.D. Tijing, J.-S. Choi, S. Lee, S.-H. Kim, H.K. Shon, Recent progress of membrane distillation using electro spun nanofibrous membrane, J. Membr. Sci., 453 (2014) 435–462.
[46] R. Beigmoradi, A. Samimi, D. Mohebbi-Kalhori, Fabrication of polymeric nanofibrous mats with controllable structure and enhanced wetting behavior using one-step electro spinning, Polymer, 143 (2018) 271–280.
[47] R. Stepanyan, A.V. Subbotin, L. Cuperus, P. Boonen, M. Dorschu, F. Oosterlinck, M.J.H. Bulters, Nanofiber diameter in electro spinning of polymer solutions: Model and experiment, Polymer, 97 (2016) 428–439.
[48] A. Amarjargal, L.D. Tijing, M.T.G. Ruelo, D.H. Lee, C.S. Kim, Facile synthesis and immobilization of Ag–TiO_2 nanoparticles on electro spun PU nanofibers by polyol technique and simple immersion, Mater. Chem. Phys., 135 (2012) 277–281.
[49] L.D. Tijing, Y.C. Woo, M.A.H. Johir, J.-S. Choi, H.K. Shon, A novel dual-layer bicomponent electro spun nanofibrous membrane for desalination by direct contact membrane distillation, Chem. Eng. Sci., 256 (2014) 155–159.
[50] C. Zhao, J. Xue, F. Ran, S. Sun, Modification of polyethersulfone membranes – A review of methods, Prog. Mater. Sci., 58 (2013) 76–150.
[51] A.M. Abdelsamad, B. Kwankhao, T.A. Gad-Allah, A.S. Khalil, M.I. Badawy, T. Bahners, M. Ulbricht, Hydrophilic polyethersulfone-based micro filtration membranes by electro spinning of polymer blends, Desal. Water Treat., 86 (2017) 89–95.
[52] N. Nasrollahi, V. Vatanpour, S. Aber, N.M. Mahmoodi, Preparation and characterization of a novel polyethersulfone (PES) ultra filtration membrane modified with a CuO/ZnO nanocomposite to improve permeability and anti-fouling properties, Sep. Purif. Technol., 192 (2018) 369–382.
[53] E.N. Şimşek, A. Akdağ, P.Z. Çulfaz-Emecen, Modification of poly(ether sulfone) for antimicrobial ultra filtration membranes, Polymer, 106 (2016) 91–99.
[54] X. Sun, Effects of the based membrane on the hydrophobicity of super-hydrophobic PES membrane and its structural properties, Mod. Appl. Sci., 4 (2010) 71–77.
[55] M. Shaban, H. AbdAllah, L. Said, H.S. Hamdy, A. Abdel Khalek, Titanium dioxide nanotubes embedded mixed matrix PES membranes characterization and membrane performance, Chem. Eng. Res. Des., 95 (2015) 307–316.
[56] A. Rastegarpanah, H.R. Mortaheb, Surface treatment of polyethersulfone membranes for applying in desalination by direct contact membrane distillation, Desalination, 377 (2016) 99–107.
[57] A.A. Khan, M.I. Siyal, C.-K. Lee, C. Park, J.-O. Kim, Hybrid organic-inorganic functionalized polyethersulfone membrane for hyper-saline feed with humic acid in direct contact membrane distillation, Sep. Purif. Technol., 210 (2019) 20–28.
[58] K. Celebi, J. Buchheim, R.M. Wyss, A. Droudian, P. Gasser, I. Shorubalko, J.-I. Kye, C. Lee, H.G. Park, Ultimate permeation across atomically thin porous graphene, Science, 344 (2014) 289–292.
[59] R. Moradi, J. Karimi-Sabet, M. Shariaty-Niassar, M.A. Koochaki, Preparation and characterization of polyvinylidene fluoride/graphene super hydrophobic fibrous films, Polymers, 7 (2015) 1444–1463.
[60] D. Roilo, P.N. Patil, R.S. Brusa, A. Miotello, S. Aghion, R. Ferragut, R. Checchetto, Polymer rigidification in graphene based nanocomposites: Gas barrier effects and free volume reduction, Polymer, 121 (2017) 17–25.
[61] D.H. Seo, S. Pineda, Y.C. Woo, M. Xie, A.T. Murdock, E.Y. Ang, Y. Jiao, M.J. Park, S.I. Lim, M. Lawn, Anti-fouling graphene-based membranes for effective water desalination, Nat. commun., 9 (2018) 683.
[62] M.S. Salem, A.H. El-Shazly, M.R. El-Marghany, M.N. Sabry, N. Nady, Effect of adding functionalized graphene on the performance of PVDF membrane in direct contact membrane distillation, Key Eng. Mater., 801 (2019) 337–342.
[63] K.-K. Yan, L. Jiao, S. Lin, X. Ji, Y. Lu, L. Zhang, Super hydrophobic electro spun nanofiber membrane coated by carbon nanotubes network for membrane distillation, Desalination, 437 (2018) 26–33.
[64] A. Abdelrasoul, H. Doan, A. Lohi, C.H.J.T.C.J.o.C.E. Cheng, Modelling development for ultra filtration membrane fouling of heterogeneous membranes with non-uniform pore size, Can. J. Chem. Eng., 92 (2014) 1926–1938.
[65] E.Y.S. Tan, S. Agarwala, Y.L. Yap, C.S.H. Tan, A. Laude, W.Y.J.J.o.M.C.B. Yeong, Novel method for the fabrication of ultra thin, free-standing and porous polymer membranes for retinal tissue engineering, J. Mat. Chem., B, 5 (2017) 5616–5622.
[66] K. Smolders, A. Franken, Terminology for membrane distillation, Desalination, 72 (1989) 249–262.
[67] M. Yao, Y. Woo, L. Tijing, C. Cesarini, H. Shon, Improving nanofiber membrane characteristics and membrane distillation performance of heat-pressed membranes via annealing post-treatment, Appl. Sci., 7 (2017) 78.
[68] F. Korminouri, M. Rahbari-Sisakht, T. Matsuura, A.F. Ismail, Surface modification of polysulfone hollow fiber membrane spun under different air-gap lengths for carbon dioxide absorption in membrane contactor system, Chem. Eng. Sci., 264 (2015) 453–461.
[69] A. Mansourizadeh, A.J. Azad, Preparation of blend polyethersulfone/cellulose acetate/polyethylene glycol asymmetric membranes for oil–water separation, J. Polym. Res., 21 (2014) 375.
[70] K.W. Lawson, D.R. Lloyd, Membrane distillation, J. Mem. Sci., 124 (1997) 1–25.
[71] M. Khayet, A. Velázquez, J.I. Mengual, Modelling mass transport through a porous partition: effect of pore size distribution, J. Non-Equil Thermody., 29 (2004) 279–299.
[72] R.W. Schofield, A.G. Fane, C.J.D. Fell, Heat and mass transfer in membrane distillation, J. Membr. Sci., 33 (1987) 299–313.
[73] M.S. Salem, A.H. El-shazly, N. Nady, M.R. Elmarghany, M.A. Shouman, M.N. Sabry, 3-D numerical investigation on commercial PTFE membranes for membrane distillation: Effect of inlet conditions on heat and mass transfer, Case Stud. Therm. Eng., 13 (2019) 100396.
[74] T. Matsuura, Synthetic membranes and membrane separation processes, CRC press, 1993.
[75] H.C. Duong, L. Xia, Z. Ma, P. Cooper, W. Ela, L.D. Nghiem, Assessing the performance of solar thermal driven membrane distillation for seawater desalination by computer simulation, J. Membr. Sci., 542 (2017) 133–142.
[76] S. Srisurichan, R. Jiraratananon, A. Fane, Mass transfer mechanisms and transport resistances in direct contact membrane distillation process, J. Membr. Sci., 277 (2006) 186–194.
[77] J. Phattaranawik, R. Jiraratananon, A.G. Fane, Heat transport and membrane distillation coefficients in direct contact membrane distillation, J. Membr. Sci., 212 (2003) 177–193.
[78] Y.C. Woo, L.D. Tijing, W.-G. Shim, J.-S. Choi, S.-H. Kim, T. He, E. Drioli, H.K. Shon, Water desalination using graphene-enhanced electro spun nanofiber membrane via air gap membrane distillation, J. Membr. Sci., 520 (2016) 99–110.

[79] F.T. Johra, J.-W. Lee, W.-G. Jung, Facile and safe graphene preparation on solution based platform, J. Ind. Eng. Chem., 20 (2014) 2883–2887.
[80] A. Akbari, M. Hamadanian, V. Jabbari, A.Y. Lehi, M. Bojaran, Influence of PVDF concentration on the morphology, surface roughness, crystalline structure, and filtration separation properties of semi-crystalline phase inversion polymeric membranes, Desal. Water Treat., 46 (2012) 96–106.
[81] N. Nady, K. Schroën, M.C.R. Franssen, M.S.M. Eldin, H. Zuilhof, R.M. Boom, Laccase-catalyzed modification of PES membranes with 4-hydroxybenzoic acid and gallic acid, J. Membr. Sci., 394–395 (2012) 69–79.
[82] Y.C. Woo, L.D. Tijing, W.-G. Shim, J.-S. Choi, S.-H. Kim, T. He, E. Drioli, H.K.J.J.o.M.S. Shon, Water desalination using graphene-enhanced electro spun nanofiber membrane via air gap membrane distillation, J. Membr. Sci., 520 (2016) 99–110.
[83] K.Y. Wang, S.W. Foo, T.-S.J.I. Chung, E.C. Research, Mixed matrix PVDF hollow fiber membranes with nanoscale pores for desalination through direct contact membrane distillation, Ind. Eng. Chem. Res., 48 (2009) 4474–4483.
[84] C. Feng, K.C. Khulbe, T. Matsuura, R. Gopal, S. Kaur, S. Ramakrishna, M. Khayet, Production of drinking water from saline water by air-gap membrane distillation using polyvinylidene fluoride nanofiber membrane, J. Membr. Sci., 311 (2008) 1–6.
[85] N. Nady, PES surface modification using green chemistry: New generation of anti-fouling membranes, Membranes, 6 (2016) 23–38.
[86] S. van der Veen, N. Nady, M.C.R. Franssen, H. Zuilhof, R.M. Boom, T. Abee, K. Schroën, *Listeria monocytogenes* repellence by enzymatically modified PES surfaces, J. Appl. Polym. Sci., 132 (2015) 41576–41582.